Mobile Doppler Radar Observations of a Tornado in a Supercell near Bassett, Nebraska, on 5 June 1999. Part I: Tornadogenesis

HOWARD B. BLUESTEIN AND CHRISTOPHER C. WEISS

School of Meteorology, University of Oklahoma, Norman, Oklahoma

ANDREW L. PAZMANY

Microwave Remote Sensing Laboratory, Department of Computer and Electrical Engineering, University of Massachusetts—Amherst, Amherst, Massachusetts

(Manuscript received 18 November 2002, in final form 28 April 2003)

ABSTRACT

This two-part paper details an analysis of high-resolution wind and reflectivity data collected by a mobile, W-band Doppler radar: The dataset captures the near-surface life history of a tornado in a supercell in north-central Nebraska on 5 June 1999. The formation of the tornado vortex near the ground is described from a sequence of sector scans ranging from 30-s intervals prior to tornadogenesis to 10–15-s intervals during much of the lifetime of the tornado.

Cyclonic vortices of 100–200 m width were found along a bow-shaped line of enhanced radar reflectivity, at what appears to have been the leading edge of a rear-flank gust front. At the time of tornadogenesis, one of these vortices was located just ahead of the nose of the bow-shaped radar echo and a jet, which were embedded within a larger-scale cyclone. At other times, small-scale cyclonic vortices coexisted with the tornado along an arc-shaped line extending to its north and northeast but did not appear to interact with the tornado. The evolution of all vortices and their associated reflectivity signatures was on a timescale shorter than 30 s, indicating that during tornadogenesis the flow pattern was highly unsteady. Mechanisms by which a smaller-scale vortex or vortices and a bow-shaped echo may have played a role in tornadogenesis are suggested. The structure of the tornado vortex near the ground, as a function of time, is discussed in Part II.

1. Introduction

Our knowledge of the dynamics of tornadogenesis in supercells is limited to a large extent by our restricted ability to observe tornadogenesis near the ground. Much of what we have learned in the last 25 years is based on Doppler radar measurements that have enabled us to visualize the wind field near tornadoes, but on spatial scales that do not explicitly resolve the tornado very well or at all. For example, early fixed-site dual-Doppler studies of tornadic storms described the parent vortex on horizontal scales of 1 km, owing to the tens of kilometers of range from the radar and half-power beamwidths on the order of 1° (e.g., Brandes 1978; Ray et al. 1981; Dowell and Bluestein 1997). Airborne single-Doppler and pseudo-dual-Doppler radar studies have resolved scales of motion down to several hundred meters, at best, when the radar-equipped aircraft has flown within 10 km of the tornado (e.g., Wakimoto and Atkins 1996; Wakimoto et al. 1998; Wakimoto and Liu 1998; Ziegler et al. 2001; Dowell and Bluestein 2002a). In both the fixed-site studies and airborne studies, high quality data are not usually available near the ground. In the case of the former, the radar beam typically passes through the tornado well above the ground, owing to the curvature of the earth. In the case of the latter, ground-clutter contamination eliminates radar coverage in the lowest several hundred meters. It is only on rare occasions that a tornado forms close enough to a fixed-site radar (e.g., Wakimoto and Martner 1992) that features well below cloud base can be analyzed on or near the tornado scale.

Other problems that limit our ability to document tornadogenesis observationally are the relatively long time intervals between volume scans (around 5–10 min) from both fixed-site and airborne radars, during which time significant evolution in low-level vortex structure may occur, and also the difficulty in capturing the entire period of tornadogenesis in a dataset. Although there have been a number of occasions on which a radar system has had the opportunity to probe a tornado, there have been much fewer occasions for a radar system to

Corresponding author address: Dr. Howard B. Bluestein, School of Meteorology, University of Oklahoma, 100 E. Boyd, Rm. 1310, Norman, OK 73019.
E-mail: hblue@ou.edu

probe a storm both just prior to and during tornadogenesis.

Ground-based, portable and mobile, X-band (3-cm wavelength) Doppler radars have been used in the last decade to determine the characteristics of the wind field in tornadoes, in large part because they can be brought close enough so that a volume relatively near the ground—that is, below 250 m AGL—can be probed and also because the spatial resolution in the cross-beam direction is maximized (Bluestein et al. 1993; Bluestein et al. 1997b; Bluestein 1999; Wurman and Gill 2000). Doppler radars with antennas having half-power beamwidths around 1° have achieved resolution on the order of 100 m, which is good enough to resolve the wind field in large tornadoes more than a kilometer across; at close ranges of several kilometers from tornadoes, a cross-beam spatial resolution as good as 50 m has been achieved.

A recent summary of what we know about tornadogenesis from observations, numerical simulations, and theory is found in Davies-Jones et al. (2001). The source of vorticity in tornadoes associated with mesocyclones in supercells is thought to be horizontal vorticity at low levels, either produced locally through baroclinic processes or imported from elsewhere; the vorticity is tilted onto the vertical and subsequently amplified by stretching underneath an updraft, driven in part by buoyancy and in part by an upward-directed perturbation pressure gradient force (Wicker and Wilhelmson 1995). The details of tornadogenesis, however, are not yet completely understood. For example, it is not known precisely how tornadogenesis is related to the mesocyclone, which is 2–5 km across and has vorticity on the order of 0.01 s^{-1}, whereas the tornado is hundreds of meters to a few kilometers across and has vorticity on the order of 0.1–1 s^{-1}; the mesocyclone is produced first aloft through tilting of deep, environmental, horizontal vorticity associated with vertical wind shear.

Several possible ways tornadoes are related to the mesocyclone have been proposed on the basis of Doppler radar observations. Wakimoto and Liu (1998), using pseudo-dual-Doppler analyses of the life history of a tornadic storm, suggested that the mesocyclone at low levels may break down into smaller-scale vortices when a downdraft is forced at its center by a downward-directed perturbation pressure gradient force that occurs when the mesocyclone becomes stronger near the ground than aloft; these smaller-scale vortices might develop from horizontal shear instabilities inside the vortex (Rotunno 1984) and then grow into tornadoes. The existence of a low-level mesocyclone, however, is insufficient by itself to produce a tornado (Trapp 1999; Wakimoto and Cai 2000).

Bluestein et al. (1997a), using a mobile, van-mounted, W-band (3-mm wavelength/95.04 GHz) Doppler radar, found evidence of 500-m scale vortices, having shear on the order of 0.05 s^{-1}, along the rear-flank downdraft gust front of a nontornadic supercell, just southeast of a kink in the gust front. It was hypothesized that similar vortices could be the seeds from which tornadoes may form.

Dowell and Bluestein (2000a,b) suggested, on the basis of airborne Doppler analyses of a cyclically tornado-producing supercell, that boundary layer horizontal vorticity is tilted into the vertical along the eastern edge of a supercell's curved updraft, which follows the rear-flank downdraft gust front/wind shift boundary. The vortex migrates westward with respect to the updraft and becomes tornadic when it reaches the rear side of the updraft, near the updraft–downdraft interface. The conceptual model of Dowell and Bluestein (2002a,b) elaborated on the conceptual model of Lemon and Doswell (1979), in which it was noted that ''the more significant tornadoes'' develop only after the mesocyclone becomes centered on the interface, separating upward and downward motion.

On the other hand, some tornadoes develop from preexisting boundary layer vortices, in the absence of a mesocyclone (Wakimoto and Wilson 1989; Lee and Wilhelmson 1997a,b). Vorticity is increased through stretching of preexisting vertical vorticity underneath growing, buoyant cumulus towers.

On 5 June 1999, a group from the University of Oklahoma (OU), in collaboration with a group from the Microwave Remote Sensing Laboratory (MIRSL) at the University of Massachusetts—Amherst (UMass), collected a high-resolution dataset that documented the entire life history of a tornado in a supercell in north-central Nebraska. The OU group used an updated version of the UMass mobile, W-band Doppler radar described by Bluestein et al. (1995, 1997a) in previous years; in 1999 the radar was mounted on a small pickup truck and a higher-resolution antenna was installed. During the 1999 spring field program, a number of supercell tornadoes were probed. The dataset collected on 5 June was the only W-band radar dataset documenting the entire life history of a tornado, beginning before the tornado had formed (Bluestein and Pazmany 2000). Some additional data were also collected by two mobile, 3-cm wavelength Doppler radar systems (Wurman et al. 1997). The purpose of this paper is to describe the evolution of the radar reflectivity and Doppler velocity structures of the portion of the storm that spawned the tornado. A description of the structure of the tornado vortex when it was mature is found in Bluestein et al. (2003, Part II of this paper).

The parent storm of the tornado is related to its larger-scale environment in section 2. In the following section, the relevant details of the radar and the characteristics of the data collected are described. Section 4 contains a detailed description of tornadogenesis as viewed by the radar. A summary of our findings, a discussion that places our results into the context of other studies, and suggestions for future work to tackle unresolved issues are found in section 5.

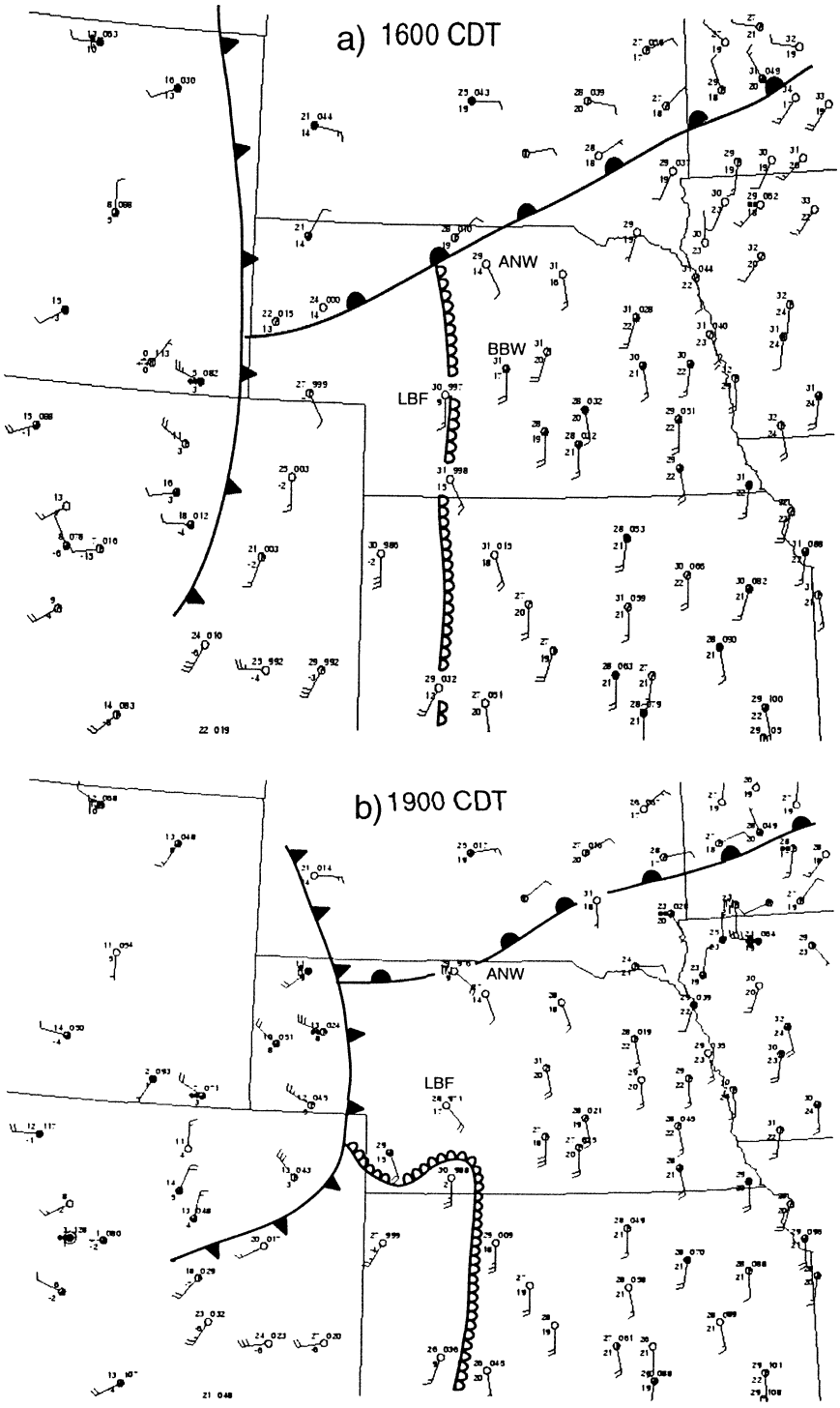

FIG. 1. Plot of surface data, centered on Nebraska, on 5 June 1999 at (a) 1600, (b) 1900, and (c) 2200 CDT. Temperature and dewpoint are plotted in °C; sea level pressure is plotted in hPa × 10, without the leading ''10'' or ''9.'' Locations of fronts are denoted by conventional symbols; location of dryline is denoted by scalloped line. LBF, BBW, and ANW denote the locations of North Platte, Broken Bow, and Ainsworth, NE (see text and Fig. 4).

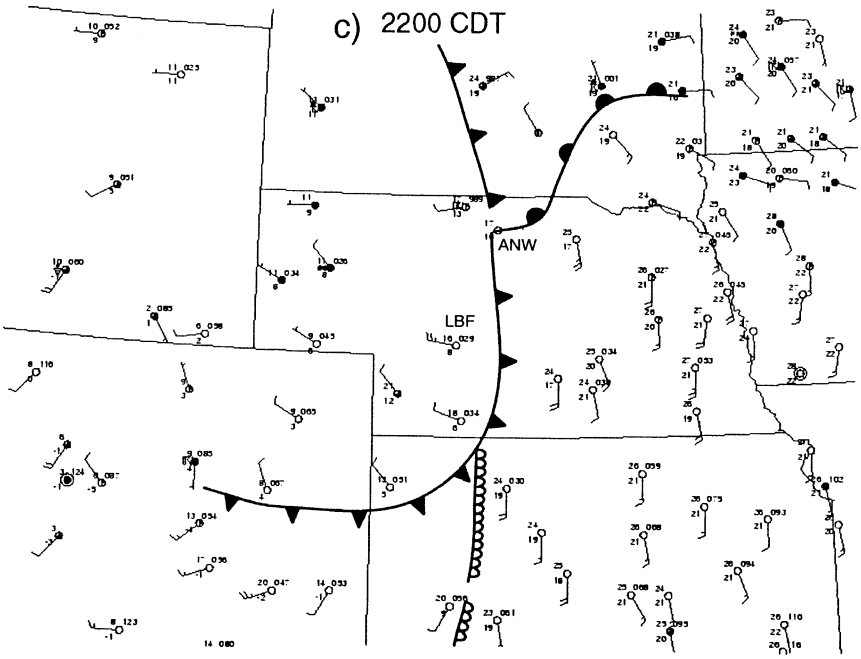

FIG. 1. (*Continued*)

2. Overview of the storm environment

To provide a context for this case study, we first describe briefly the synoptic and mesoscale environment of the parent supercell storm that spawned the tornado. Convective storms were initiated [see the Next-Generation Weather Radar (NEXRAD) National Reflectivity Mosaic at the National Climatic Data Center (NCDC) Web site] between 1600 and 1700 CDT (all times are given in CDT; UTC is 5 h later), southwest and west of North Platte, Nebraska, near a dryline that extended southward into western Kansas (Fig. 1a). At the same time, a stationary/warm front stretched from southeastern South Dakota, west-southwestward, across north-central Nebraska to the Nebraska Panhandle–Wyoming border, and a cold front was progressing eastward and southeastward in northeastern Colorado and eastern Wyoming. While the convective storms were moving northward or north-northeastward through west-central Nebraska, the dryline retreated westward (Fig. 1b), and surface winds backed in the moist air mass east of the dryline. The cold front progressed eastward and between 1900 and 2200 caught up to the dryline in central Nebraska, south of the stationary/warm front (Fig. 1c).

The environment of the convective storms, estimated from the 1900 sounding at North Platte (Fig. 2), had substantial convective available potential energy (CAPE) ($\sim$2500–3000 J kg^{-1}; the latter estimate is for a surface parcel and the former estimate is for an average parcel from the lowest 500 m) and vertical shear in the lowest 6 km (30 m s^{-1}/6 km), necessary conditions for the production of supercells when an isolated storm is triggered in a homogeneous environment (Weisman and Klemp 1982). The backing of the surface winds with time likely was in response to synoptic-scale forcing from an intense, closed-off low pressure area/trough at 500 mb (Fig. 3), which was approaching from the west (and located over western Colorado at 1900). The increase in southwesterly winds at 500 mb with the approaching trough and the backing of the surface winds led to increasing vertical wind shear during the late afternoon hours.

At 1922 the National Weather Service (NWS) issued a severe thunderstorm warning for a cell 16 km south of Moon Lake (about 45 km southwest of Ainsworth, Nebraska; see Fig. 4), moving to the north at 11 m s^{-1}. It was from this storm that a tornado subsequently developed. (It is noted, however, that the motion of the tornado and its parent storm after 1922 was actually to the northeast.) It is not believed that the storms prior to this time exhibited supercell characteristics, based on limited visual observations, mobile Doppler radar data (to be noted subsequently), and the lack of severe thunderstorm or tornado warnings; however, the area in which the storm became tornadic was unfortunately located 150–200 km from the nearest Weather Surveillance Radar-1988 Doppler (WSR-88D) (at North Platte) (Fig. 4), thus precluding a detailed, high-resolution analysis of the evolution of the low-level structure of the parent storm. However, radar images from a set of mobile, 3-cm-wavelength Doppler radars, the Doppler on Wheels (DOW2 and DOW3) (Wurman et al. 1997), which were moving northward along State Highway 7, south of Ainsworth, with the storm located to their northwest (Fig. 4), provided a close-range look at the

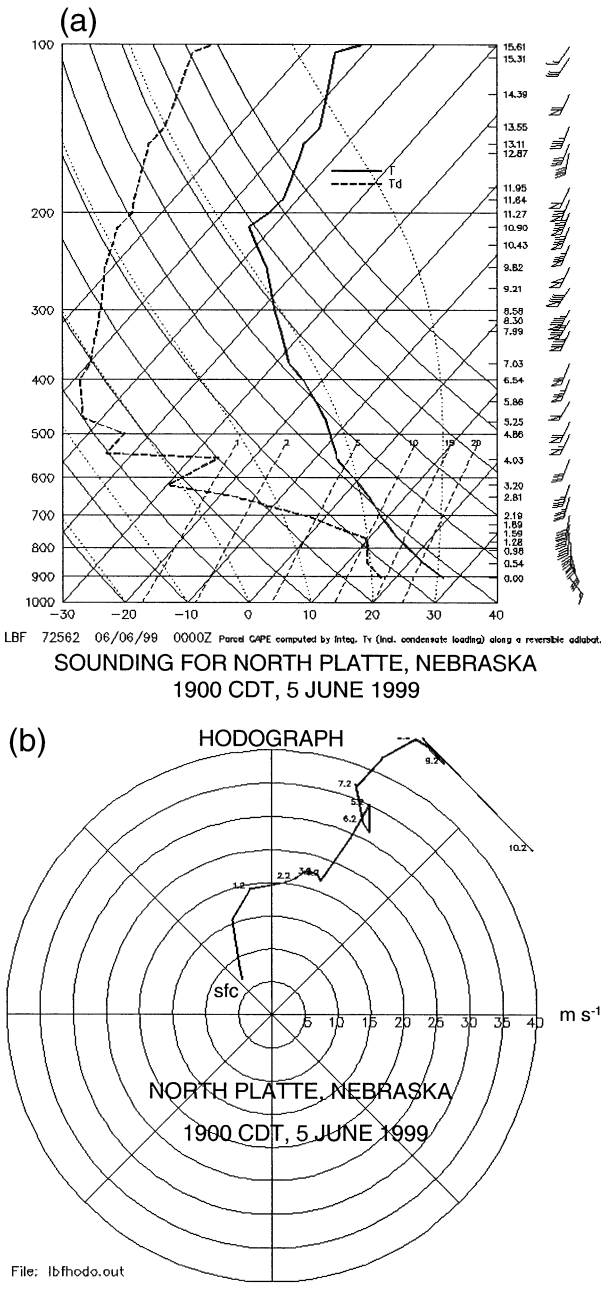

FIG. 2. (a) Sounding at North Platte, NE, on 5 Jun 1999 at 1900 CDT. (a) Temperature (solid line) and dewpoint (dashed line) profiles (°C) plotted on a skew *T*–log*p* diagram along with the winds at the right. Half barb, full barb, and pennant represent wind speeds of 2.5, 5, and 25 m s^{-1}, respectively. Heights (km AGL) are also plotted at the right; pressure in hPa is plotted at the left. Sloping dashed lines are water vapor mixing ratio, labeled in g kg^{-1}. Dotted lines indicate selected moist adiabats. (b) Hodograph with wind speeds given in m s^{-1} and heights indicated in km AGL.

storm prior to tornadogenesis and will be discussed in section 4.

The tornado formed around 2012, before its parent storm had arrived at the warm front, which was located along and north of the Nebraska–South Dakota border (Fig. 1b). Atkins et al. (1999) have shown, using numerical simulation experiments, how low-level mesocyclogenesis can be hastened when a supercell interacts with a preexisting thermal boundary. It thus appears, however, that in this case there was no significant interaction of the parent storm with the warm front boundary at the time of tornadogenesis.

3. The W-band, mobile Doppler radar: Characteristics and data collected

The most valuable characteristic of the UMass W-band radar system is its fine spatial resolution: the half-power beamwidth of its antenna is only 0.18°, which yields a cross-beam resolution of 10 m at 3.2-km range. With such a narrow beam the radar can scan closer to the ground, with less ground-clutter contamination than radars operating at longer wavelengths that have wider-beam antennas. The range resolution, which is determined by the length of the radar pulses (100 ns), is 15 m. The radar is thus well capable of resolving the structure of vortices down to scales of 50–100 m, within 100 m of the ground.

Although the maximum unambiguous Doppler velocity is only ± 12 m s^{-1} in conventional pulse-pair mode [for a pulse repetition frequency (PRF) of 15 kHz], in polarization diversity pulse-pair (PDPP) mode the maximum unambiguous Doppler velocity is ± 79 m s^{-1}; such a high maximum unambiguous velocity allows one to estimate the winds in tornadoes without encountering serious difficulties unfolding aliased velocity data. The reader is referred to Doviak and Sirmans (1973) and Pazmany et al. (1999) for details on how PDPP works and how it was implemented in the UMass radar. The PDPP technique, however, does not work when the targets are within about 1.5-km range, owing to the finite polarization isolation of the switch network and the antenna, and provides noisier estimates than the conventional pulse-pair technique. Generally the radar is not operated within 1.5 km of a tornado for safety considerations anyway. Beyond 1.5-km range, when the PDPP data are too noisy, the PDPP data can be used to unfold the less noisy conventional pulse-pair data.

The maximum unambiguous range of the radar system is 10 km, which is near the close side of the upper limit for how far tornadoes can be seen clearly if there is not too much intervening rain; typically a tornado at a range of 3 km is well visible, unless there is intervening heavy precipitation, and is safe to observe. Since W-band radars are subject to more severe attenuation than radars operating at longer wavelengths, range folding from targets beyond 10 km is generally not a problem. Furthermore, it has been our experience that in heavy precipitation, much of the signal is attenuated substantially beyond 3–5 km. So, observing tornadoes at a range of about 3 km is considered optimum.

Because the wavelength of the W-band radar is much shorter than that of radars operating at X, C, and S

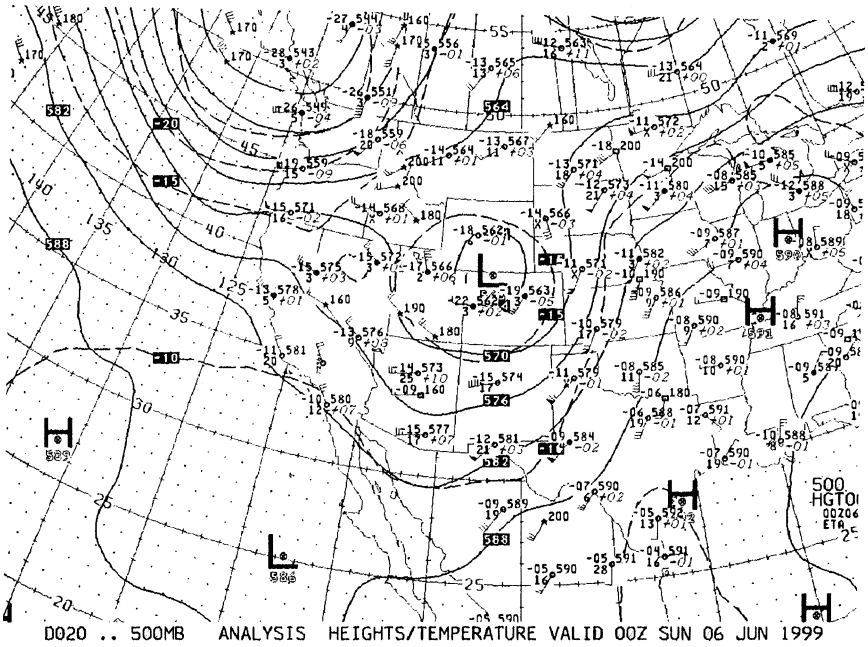

FIG. 3. Analysis of the height field (dam) at 500 hPa at 1900 CDT. Temperature (°C) and 500-hPa height (dam) plotted; wind barbs as in Fig. 2. National Centers for Environmental Prediction (NCEP) map, archived by the NCDC.

bands, the sensitivity to small scatterers is greater. For cloud droplets, raindrops, and hailstones, the scattering is in the Mie range (Lhermitte 1990) rather than in the Rayleigh range. It is difficult to estimate the rainfall rate from the radar reflectivity mainly owing to severe attenuation and to our lack of knowledge of the drop-size distribution and its relation to the reflectivity; however, measurements of Doppler velocity are not affected by the Mie scattering. Since the scattering is in the Mie range and since the attenuation at W band is extreme, reflectivity data must be interpreted in a qualitative manner only, and with caution.

The reader is referred to Bluestein (1999) for a description of storm-intercept strategies and procedures common to earlier experiments, which we followed during the 1999 field experiment. On 4 June 1999, the storm-intercept team spent the night at North Platte and on 5 June, it traveled to Broken Bow, Nebraska, to be positioned for field operations after convective storms had been initiated (Fig. 4). The storms that formed southwest of North Platte during the afternoon tracked to the north-northeast into a large road void (approximately 70 km by 70 km) southwest of Ainsworth (Fig. 4). We reached Ainsworth via State Highway 7 (which bounds the road void to the east) from Brewster and Dunning, Nebraska, and stopped, just east of town, to observe the storm approaching us from the southwest. We had three main deployment sites: east of Ainsworth from 1915–1954, east of Long Pine, Nebraska, from 2003–2016, and west of Bassett, Nebraska, from 2017–2019 CDT. The deployment times are estimated to be good to within about ±1 min. Data were collected in between the last two deployments while the radar truck was moving to the east, to avoid hail which was approaching from the west and to minimize the effects of attenuation by intervening precipitation. The radar was pointed to the south-southwest through south to south-southeast. No useful data were collected during the first deployment when precipitation obscured cloud base and no vortex signatures were evident, or during subsequent deployments after 2019 when another tornado formed to our northeast but was located beyond 10-km range. The focus of this paper is on data collected between 2007 and 2019, from a time before the tornado formed to a time when it was dissipating.

Data were collected at the lowest elevation angle possible above the visible terrain in sector scans, at approximately 30-s intervals initially, before a tornado had formed, and at approximately 10–15-s intervals later on, when the tornado was visible. The time of each scan hereafter referred to in the text and in the figures (in hours, minutes, and seconds) is that of the beginning of each sector scan. The spatial bounds of the sector scans were determined by viewing real-time color images from a bore-sighted video camera mounted on the radar antenna. Before the tornado had formed, the scans covered a relatively wide sector to include all features near a visible cloud base approaching from the south-southwest (not shown) thought to contain a rotating updraft and wall cloud. Owing to curtains of precipitation and other intervening areas of rain and/or hail, it was not certain initially that the radar antenna was aimed at pre-

cisely the correct direction to capture tornadogenesis. After the tornado's condensation funnel had formed, fortunately within the sector being scanned, the bounds of the subsequent sector scans included all of the condensation funnel, a near-surface debris cloud, and areas just to the right and left of the debris cloud. Scans at other elevation angles (volume scans) were not taken to minimize the time between scans at the same elevation angle; information about the vertical structure of the tornado is therefore not available for this case study: spatial coverage was sacrificed for the sake of temporal resolution.

The data were stored on both the radar computer's hard disk in the radar truck and on tape. At MIRSL the data were converted into universal format files and viewed at OU using the National Center for Atmospheric Research's SOLO software package (Nettleton et al. 1993).

4. Description of tornadogenesis as viewed by the Doppler radar

a. Overall radar reflectivity structure prior to and during tornadogenesis

In this section we describe the sequence of radar observations prior to and during tornadogenesis. There are no generally accepted criteria for when a vortex becomes a tornado. It is therefore not exactly clear at what second the tornado on 5 June 1999 actually began. When the highest ground-relative wind speeds were only around 10–15 m s^{-1} and there was no debris cloud or condensation funnel, the tornado had certainly not yet formed; when a rotating debris cloud at the ground appeared and the highest wind speeds were in the F0 range on the Fujita (1981) scale (18–32 m s^{-1}) or higher, even though there was still no condensation funnel, a weak tornado is thought to have formed.

Prior to tornadogenesis and when the storm was beyond the range of the UMass W-band radar, low-elevation-angle (at 500 m and below) observations were available sporadically from each of the DOW radars while they were in transit (Fig. 4). At 1938 (recall that a severe thunderstorm warning had been issued by the NWS based on WSR-88D observations at 1922), the storm had a narrow (approximately 1 km wide) appendage on its southeast side (Fig. 5a, right). At this time, DOW3 was located (Fig. 4) about 14 km to the southeast of a kink in the appendage. Without quantitative knowledge of the orientation of the radar truck and its motion, it is not possible to determine the ground-relative or storm-relative Doppler wind fields precisely. However, since the DOWs were located on an approximately north–south stretch of State Highway 7 south of Ainsworth and heading northward at approximately 30 m s^{-1}, the zone of strong gradient in Doppler velocity (about 30 m s^{-1} change over 5 km or less) that follows the appendage (Fig. 5a, left) is consistent with a wind shift across it. Along the northwest–southeast-oriented portion of the appendage, which was aligned approximately along a radial, there was cyclonic shear in the Doppler velocity (white and a few yellow splotches to the right of the appendage, adjacent to green to the left of the appendage); along the north-northeast–south-southwest-oriented portion of the appendage, which was aligned substantially at constant range, there was convergence in the Doppler velocity (yellow at ranges closer than the appendage, green at ranges beyond the appendage). At 1950, DOW2, which was crossing the appendage, was located approximately 7 km south-southeast (Fig. 4) of the right-angle bend in it (Fig. 5b, right), seen in Fig. 5a 12 min earlier.

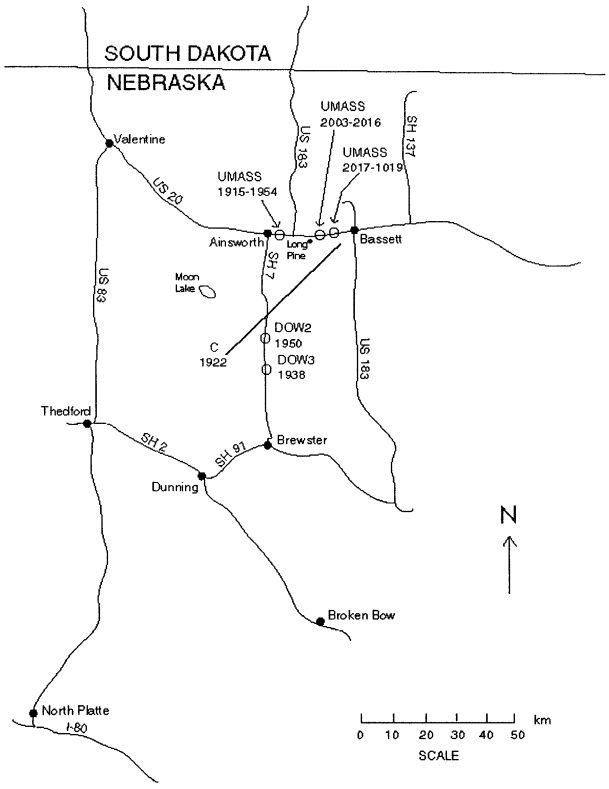

FIG. 4. Map centered in north-central Nebraska. Major cities and towns, highways, approximate locations and times (CDT) of deployments of UMass W-band radar, of DOW2 and DOW3 at a few selected locations and times (CDT), the core of the storm at 1922 CDT (''C'') as indicated by NWS Doppler radar at North Platte, and the approximate track of the tornado and its pre-tornado vortex features (solid diagonal line) are indicated.

At 2007:42 a cusp or inflection point or kink in a line of enhanced reflectivity at 8–8.5-km range was moving toward the radar (Fig. 6). This radar-echo cusp is similar to that found in the Grand Island, Nebraska, tornadic storm of 3 June 1980 (Fujita 1981, his Fig. 12), and elsewhere, and in other cases was coincident with the ''occlusion point'' of the rear-flank downdraft gust front with the forward-flank downdraft gust front (Lemon and Doswell 1979, their Fig. 7), at the tip of the hook echo

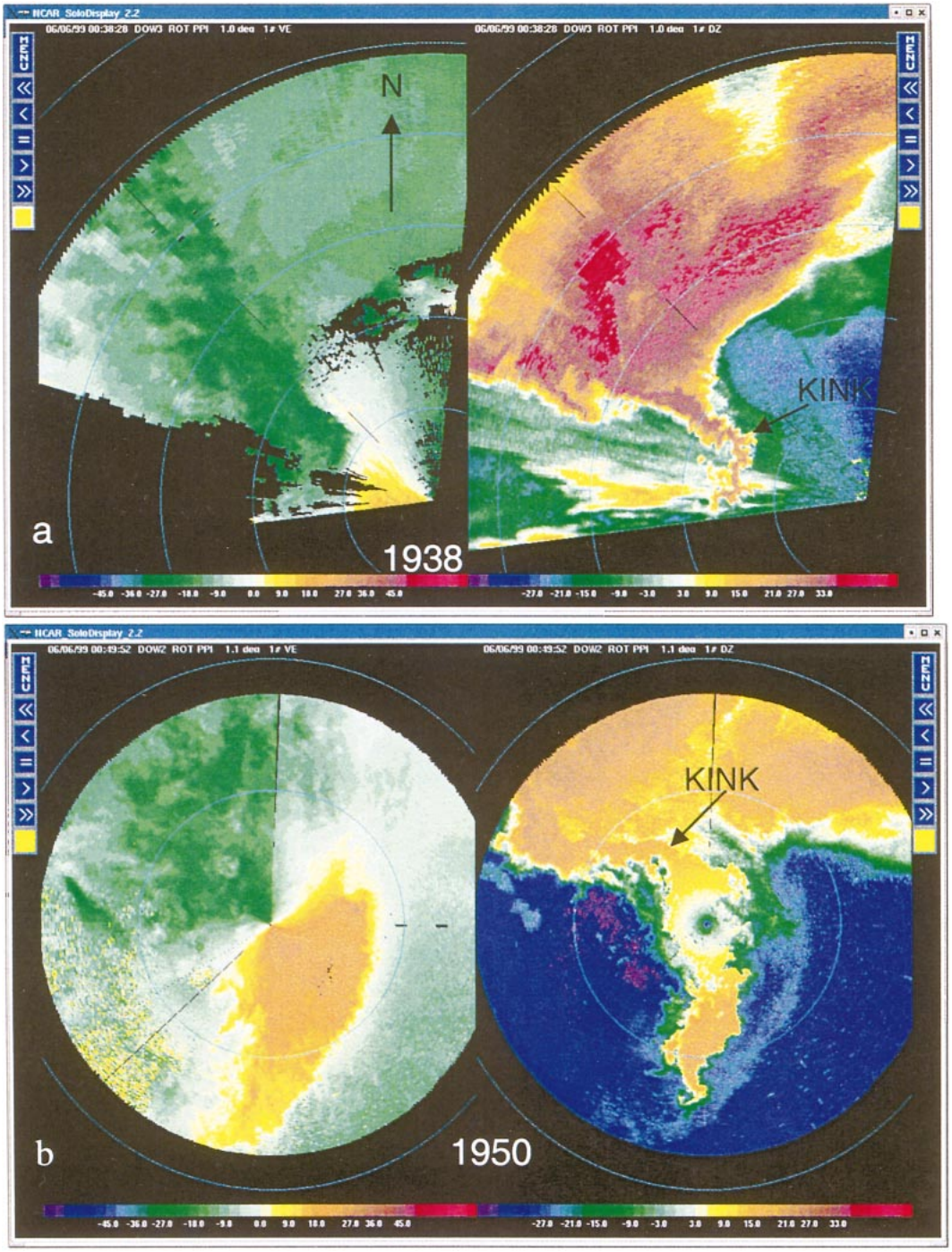

FIG. 5. Unfolded, truck-relative (DOW trucks were moving approximately northward) (left) Doppler velocity in m s^{-1} and (right) radar reflectivity in dBZ from (a) DOW3 at 1938 CDT and (b) DOW2 at 1950 CDT, south of Ainsworth, NE, on State Highway 7 (see Fig. 4). Constant-range circles are shown at 10-km intervals.

(Markowski 2002). The cusp is probably the same feature as the kink in the appendage, as seen by the DOWs 15–20 min earlier (Fig. 5). The radar-echo cusp was characterized by weak cyclonic shear in the Doppler velocities (not shown). By 2008:57 the cusp had assumed the configuration of a 500-m-wide bow-shaped echo, having enhanced reflectivity along its leading edge; the bow-shaped echo crossed the 7-km range marking at 2009:24. The enhanced reflectivity is evidence that the number of radar scatterers per unit volume increased, which is consistent with an increase in convergence along the gust front; it is also possible that the

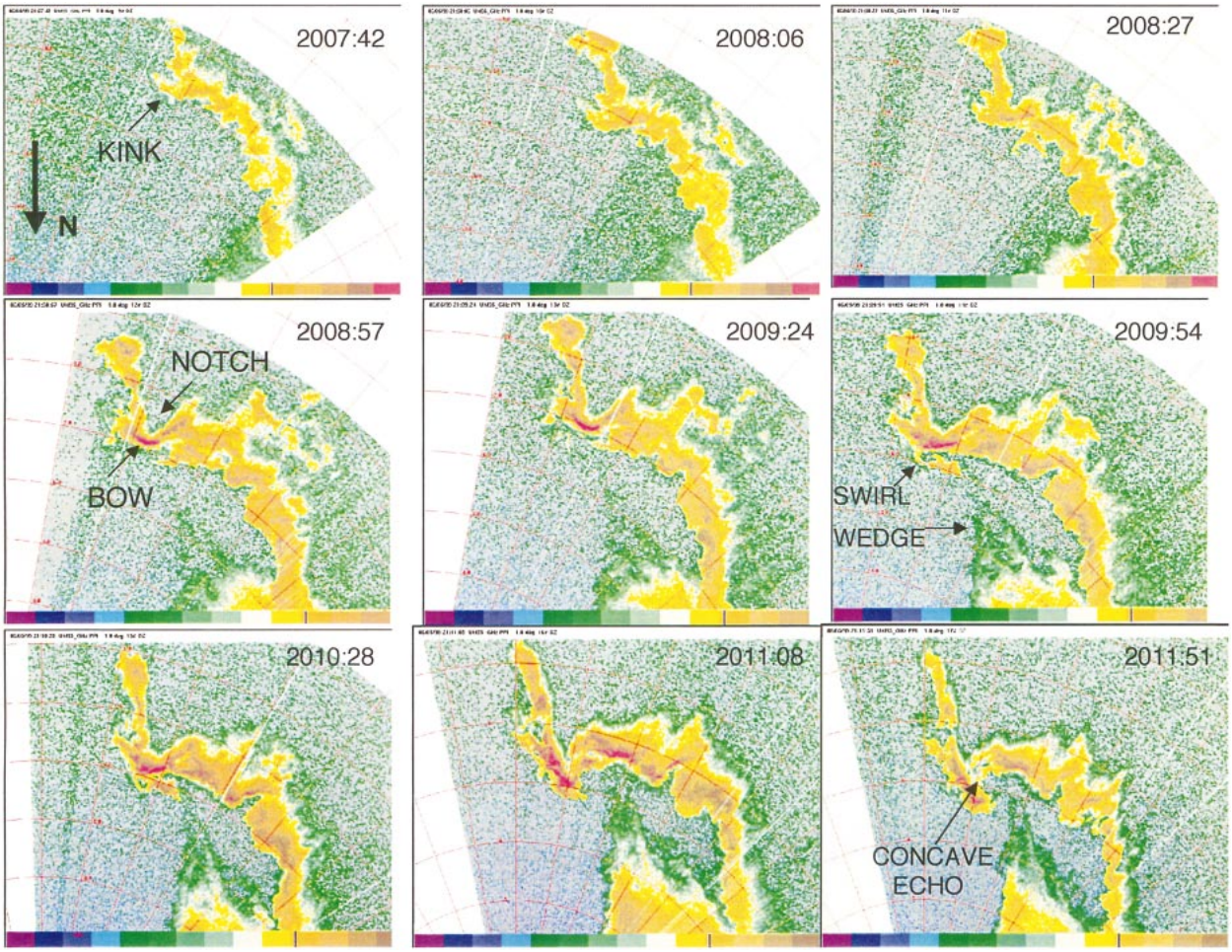

FIG. 6. Radar reflectivity field (as viewed by the W-band radar) before and during tornadogenesis, from 2007:42 to 2011:51 CDT. Absolute reflectivity scale is not shown. Reflectivity increases to the right (−30 dB*Z* at extreme left, 20 dB*Z* at extreme right) for the color scale shown below each panel. Red lines are range markings every km in range and every 10° in azimuth. The radar was stationary during this time period and was looking off to the south and southwest. Some features described in the text are pointed out at selected times.

precipitation rate increased locally or the size of the scatterers increased, though it is not clear why they would have done so locally. The radar return in the reflectivity notch behind the bow-shaped echo was too weak to permit the estimation of the Doppler velocity field there; perhaps if the length of the radar pulses had been increased, as they are in clear-air mode, it would have been possible to estimate the convergence along the gust front.

At 2009:54 a cyclonic swirl about 400 m across appeared just ahead of the leading edge of the bow-shaped radar echo. It continued to spiral around in a cyclonic fashion at 2010:28, but by 2011:08 it had disappeared, while the cusp began to show evidence of larger-scale cyclonic rotation, as a semicircle of concave echo appeared just to the right of the leading edge of the bow-shaped echo. Echoes of a more uniform appearance moved outward from the radar toward the area east of the concave echo (see the wedge-shaped echo moving upward from the bottom center of the radar images; Fig. 6). At 2011:51 the concave echo had wrapped up into almost three-fourths of a circle about an echo-free area around 5 km in range. By 2012:35 the bow-shaped echo had completely spiraled around, leaving behind an elliptically shaped, echo-weak/free hole (Fig. 7). The wedge-shaped radar echo, which was noted earlier, was now aimed at the region just to the right of the hole. Echo-weak holes in tornadoes are apparently ubiquitous, having been noted, for example, by Fujita (1981), Wakimoto and Martner (1992), Wurman and Gill (2000), Bluestein and Pazmany (2000), inferred by Bluestein et al. (1993), and seen often in other mobile radar datasets of tornadoes.

During the latter time periods, the OU group viewed a cloud base to its south, under which a funnel cloud appeared intermittently amidst cyclonically rotating precipitation curtains. The motion of some precipitation elements appeared to have a strong component from right to left, that is, toward the east. The area to the west of the rain curtains was relatively bright. This rap-

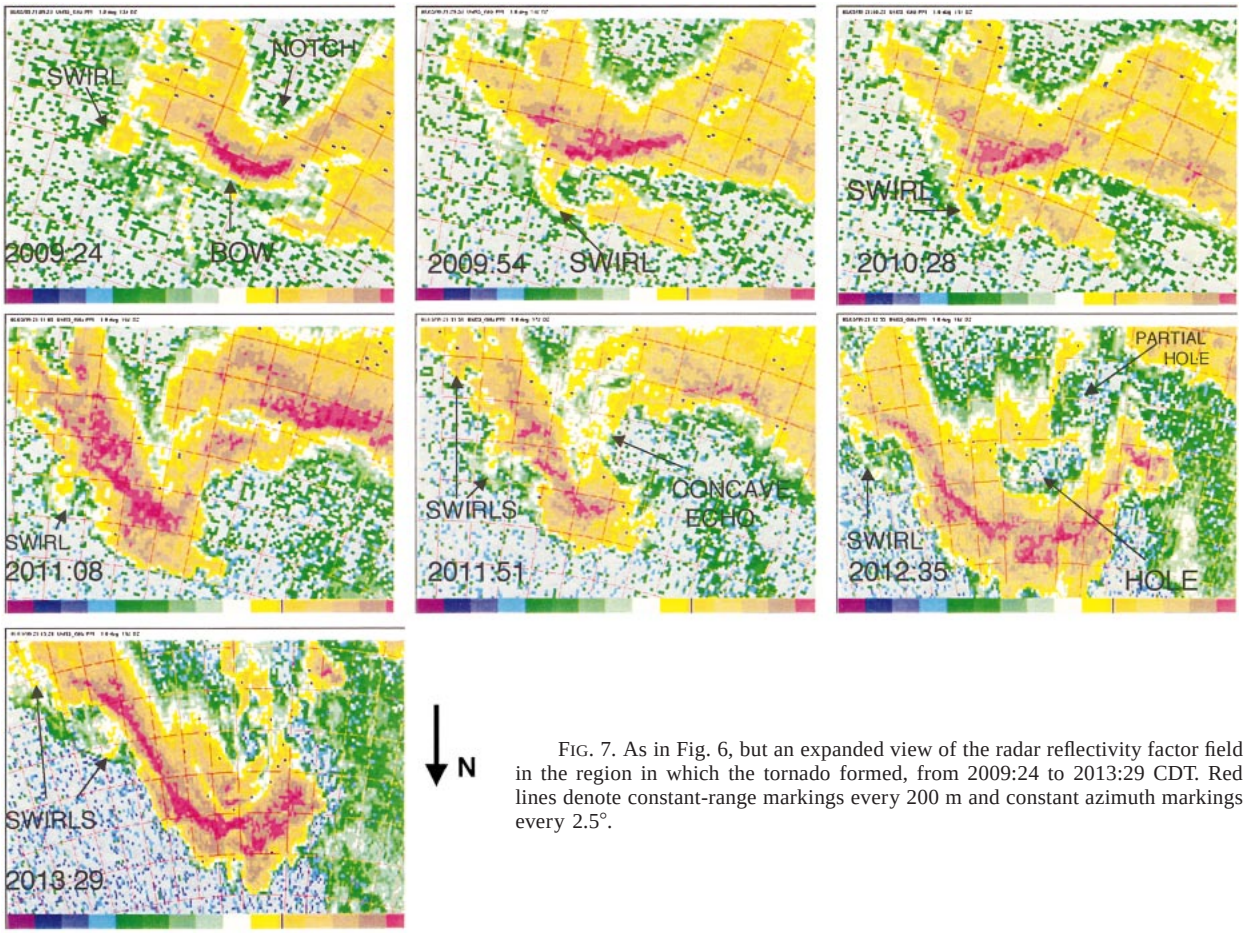

FIG. 7. As in Fig. 6, but an expanded view of the radar reflectivity factor field in the region in which the tornado formed, from 2009:24 to 2013:29 CDT. Red lines denote constant-range markings every 200 m and constant azimuth markings every 2.5°.

idly eastward moving current of air, under a relatively bright sky, is consistent with the conceptual model of the rear-flank downdraft and clear slot in a supercell (Lemon and Doswell 1979; Markowski 2002), though we have no storm-scale Doppler observations to confirm this interpretation (the DOWs were moving at this time, and furthermore the air motions behind the rear-flank gust front would have been predominantly normal to its radar beams if they had been collocated with the UMass radar).

b. Expanded view of tornadogenesis and other vortices

The reader is referred to Figs. 7 and 8 for the following discussion. At 2009:24 Doppler signatures of cyclonic vortices were found at the swirl in reflectivity approximately 600 m to the left of the nose of the bow-shaped echo (cf. also Fig. 6) and just to the right of the bow-shaped echo. Each vortex signature was around 100 m across (i.e., the approximate distance between the maximum in Doppler velocity and the minimum in Doppler velocity was around 100 m; the scale of the vortex itself must have been wider, perhaps twice as wide; in this paper the size of a vortex is measured by the distance between Doppler velocity extrema). Along the nose of the bow-shaped echo there was a jet in approaching velocities (green flanked by yellow- and/or orange-coded Doppler velocities), ahead of the echo-weak notch.

At 2009:54 the reflectivity swirl located to the left of the nose of the bow-shaped echo was no longer visible, but a new one appeared just ahead of the nose of the bow-shaped echo. It is possible that the swirl at 2009:54 was the same one seen to the left of the bow at 2009:24. However, between 2009:54 and 2010:28, the swirl remained at the nose of the bow, so that it is more likely that a new swirl had formed. The region of cyclonic shear associated with the swirl just ahead of the bow-shaped echo was about 200 m across at 2010:28, remaining distinct from the region of broader, convergent, cyclonic shear (Brown and Wood 1991) around 600 m across. Dowell and Bluestein (2002a) found, in their airborne Doppler analysis of tornadogenesis of the 8 June 1995 storm near McLean, Texas, that one of the tornadoes was off to the side of the larger-scale mesocyclone (see their Fig. 7), from which it may be inferred that there were vortices of two distinct scales and

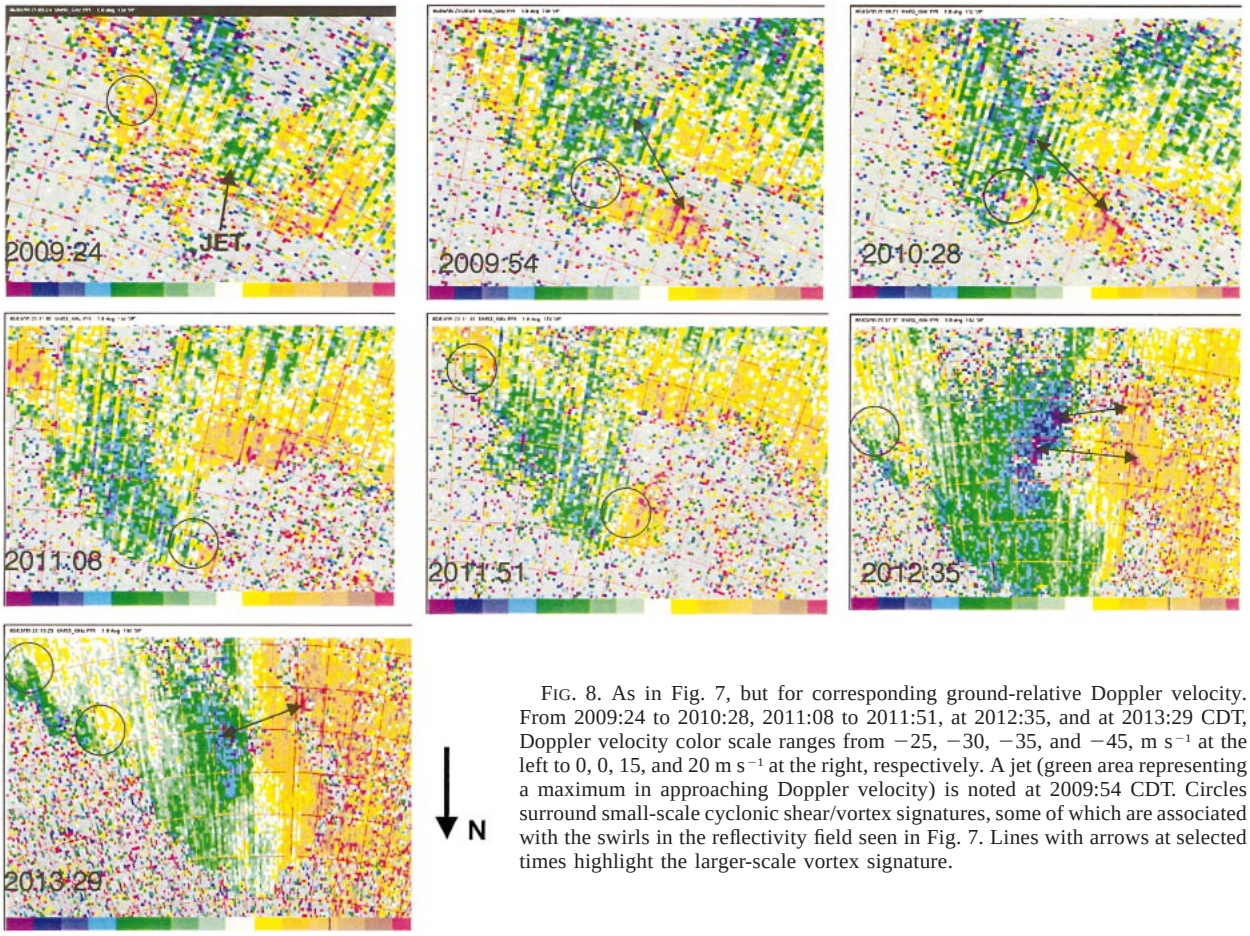

FIG. 8. As in Fig. 7, but for corresponding ground-relative Doppler velocity. From 2009:24 to 2010:28, 2011:08 to 2011:51, at 2012:35, and at 2013:29 CDT, Doppler velocity color scale ranges from −25, −30, −35, and −45, m s^{-1} at the left to 0, 0, 15, and 20 m s^{-1} at the right, respectively. A jet (green area representing a maximum in approaching Doppler velocity) is noted at 2009:54 CDT. Circles surround small-scale cyclonic shear/vortex signatures, some of which are associated with the swirls in the reflectivity field seen in Fig. 7. Lines with arrows at selected times highlight the larger-scale vortex signature.

that the overall structure was not symmetric about the center of the mesocyclone. In our case, there was evidence of two vortices, a smaller-scale one embedded within a larger-scale one. Trapp (1999) has noted several instances of tornadogenesis during VORTEX in which the tornado appeared on the periphery of the mesocyclone, not in the center.

At 2011:08, another swirl in reflectivity appeared to the left of the bow-shaped echo. The leading edge of the bow-shaped echo was characterized by a broad region of cyclonic shear about 500–600 m across and a smaller-scale cyclonic shear signature was located at the leading edge of the bow-shaped echo; the intensity of the former signature may be underestimated because there were relatively few visible radar scatterers just to the east of the leading edge of the bow shaped echo. As the region to the right of the leading edge of the bow-shaped echo assumed a more concave shape at 2011:51, the cyclonic-vortex signature around 500 m across became better defined. By 2012:35, when the concave echo had closed off to form an echo-weak hole, a strong cyclonic vortex signature with around 50 m s^{-1} difference in Doppler velocity across the dipole in velocity extrema was noted; the extrema were separated by about 500 m. Since the approaching wind speeds were 35 m s^{-1} and a vortex signature was evident, it is likely that a tornado had formed over the previous 30-s period. In addition, there was a partially closed-off weak-echo hole and associated vortex couplet located just 200–300 m away to the south, adjacent to the tornado vortex. The scan rate was not fast enough to detect the temporal continuity of each separate vortex.

At 2012:35 a swirl in reflectivity accompanied by a cyclonic vortex signature around 200 m across, around 800 m to the left of the leading bulge in the radar echo, was also noted. At 2013:29 two swirls and cyclonic vortex signatures were still evident to the left of the nose of the bow; the swirls and vortex signatures were still about 200 m across. The vortex signature associated with the tornado was now about 400 m across and located about 400 m behind and just to the right of the leading edge of the bow-shaped echo.

At 2014:04 the cyclonic swirl to the left of the leading bulge in the radar echo was even more intense; it now had a shear of about 30 m s^{-1} across 100–150 m (Fig. 9). The swirl closed off, while maintaining its intensity at 2014:42, about 700 m to the left of the leading edge of the bow-shaped echo. A band of cyclonic shear (pur-

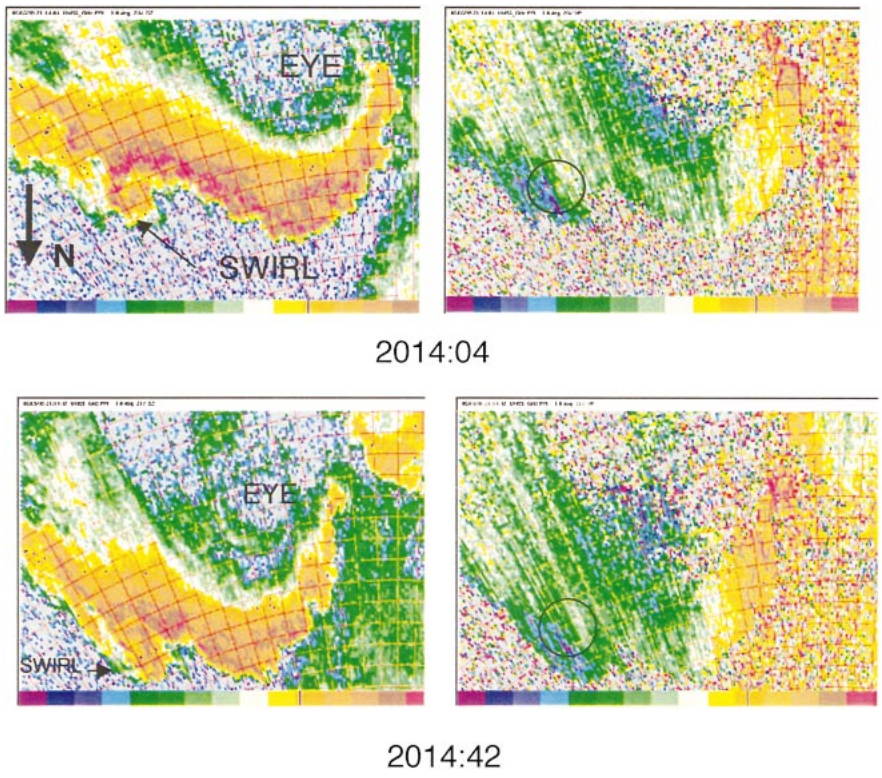

FIG. 9. As in Figs. 7 and 8, but at 2014:04 and 2014:42 CDT, centered on area of bulge in rear-flank gust front, where small-scale vortices/swirls were found. (left) Reflectivity and (right) ground-relative Doppler velocity are shown. Red lines denote constant-range markings every 100 m and constant azimuth markings every 2.5°. Circles surrounding the vortex signature (purple–blue to green–white) associated with the swirl seen in the reflectivity panels on the left-hand side can be seen on the right-hand sides.

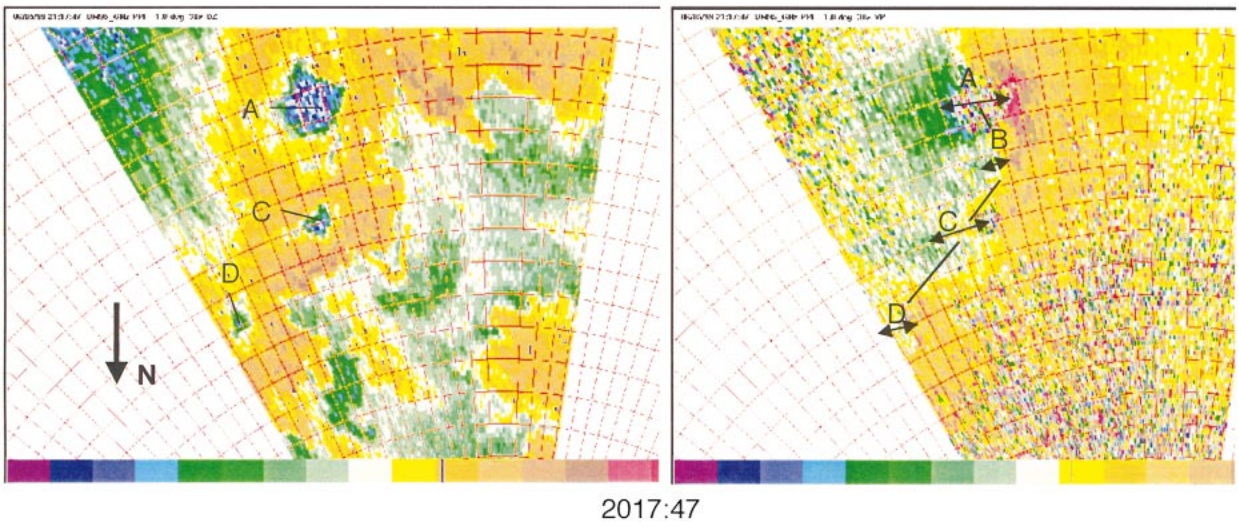

FIG. 10. (left) Radar reflectivity factor and (right) ground-relative Doppler velocity at 2017:47 CDT. Constant-range and azimuth markers (red) are shown every 100 m and 2°, respectively. Doppler velocity scale ranges from -60 m s^{-1} at the left (purple) to 20 m s^{-1} (red) to the right. Vortex signatures are located at A (the tornado), B, C, and D. Arc-shaped line connects vortex signatures A–B–C–D.

ple–blue to green–white) is seen not only with the swirl but also all along the leading edge of the reflectivity band. Thus, the swirl represents a maximum of cyclonic vorticity embedded within a cyclonic shear zone. The swirl appears to be qualitatively similar to the swirls documented along the rear-flank gust front in a supercell during the 1995 Verification of the Origins of Rotation in Tornadoes Experiment (VORTEX-95) (Bluestein et al. 1997a). In the 5 June 1999 case, however, all the swirls were curled in a counterclockwise manner and the Doppler shear was cyclonic; in the VORTEX case there was also a nearby clockwise-curled swirl having anticyclonic vorticity that was a member of a counter-rotating vortex couplet.

Evidence of other vortices along the band of cyclonic shear is seen later on north-northeast of the tornado (Fig. 10). Vortex signatures C and D are associated with echo-weak holes, while vortex signature B is not. Vortex signature A is associated with the tornado and a weak-echo hole. The spacing between adjacent vortex signatures is between 250 and 400 m. The line connecting the vortex signatures A–B–C–D forms an arc. A line of similar vortex signatures might have been present at other times, but the radar did not scan a wide-enough sector to view more than just a few of them.

5. Summary and discussion

An intriguing finding of this study is that vortices of two scales can coexist and may interact during tornadogenesis. Cyclonic vortices of only 100–200-m scale along the rear-flank gust front were found, one of which, *when located just ahead of a small-scale nose (associated with a bow-shaped radar echo) in the rear-flank gust front, apparently was absorbed by a larger, 500-m-''scale'' vortex as a tornado was forming.* Other small-scale vortices were found along the rear-flank gust front later, but none of them developed into tornadoes. Since the evidence that the two vortices of different scale interacted during tornadogenesis is only circumstantial, other case studies must be analyzed to see if vortex interaction is indeed necessary for tornadogenesis, or if it was just a coincidence in this case.

The interaction of vortices of different origin during tornadogenesis is a process that has been described for larger-scale vortices. Ziegler et al. (2001), for example, in a pseudo-dual-Doppler analysis of airborne Doppler radar data from the Newcastle–Graham, Texas, storm of 29 May 1994, found that a shallow boundary layer mesocyclone existed separately from a mesocyclone that built downward with time. Our dataset has the serious limitation that data at only one level were available. We can only speculate that the smaller-scale vortices may have been present only in the boundary layer, while the larger-scale vortex was associated with the mesocyclone, since the latter was coincident with the hook echo and echo kink.

All vortices evolved rapidly during tornadogenesis; significant changes in appearance of the vortices and their associated reflectivity signatures occurred on timescales shorter than 30 s, so that it was frequently difficult to establish the temporal continuity of each vortex: The wind field during tornadogenesis was highly unsteady.

Since the timescale of vortex interaction was on the order of only a few tens of seconds or less, very rapidly scanning radars are necessary to resolve vortex interaction. Numerical modeling studies must be able to reproduce features having scales as short as 10 m or less; large-eddy simulations (Lewellen and Lewellen 1997) are probably required to reproduce the small-scale vortices and to assess what the necessary conditions are for their formation. Barotropic instability due to the roll-up of vortex sheets (Drazin and Howard 1966; Barcilon and Drazin 1972) along the rear-flank gust front is a likely candidate source mechanism. The source of vorticity along the rear-flank gust front could be the tilting of streamwise horizontal vorticity, as described by Dowell and Bluestein (2002b).

Because the small-scale bow-shaped echo preceded tornadogenesis by only several minutes, it is speculated that it might have induced tornadogenesis through ''corner-flow collapse'' (Lewellen and Lewellen 2002). In this process, a sudden change in near-surface inflow (Lewellen et al. 2000b), such as the impinging of a narrow, jetlike downdraft (which may have been responsible for producing the bow-shaped echo) on the larger-scale vortex, initiates intensification at the surface (much more rapidly than a larger-scale vortex can intensify aloft). Lewellen et al. (2000a) have demonstrated that the vortex corner flow is sensitive to the near-surface inflow. Since current high-resolution mobile radar systems do not scan rapidly enough, it is believed that numerical experiments are necessary to test the corner-flow collapse hypothesis.

Acknowledgments. We are indebted to the following OU graduate students for the assistance we received during the field experiment in which the data for this study were collected: Greg Lehmiller, Peter Leptuch, and David Dowell. They shared the driving and assisted in making real-time decisions. Erik Rasmussen (NSSL/CIMMS) provided nowcasting support. Josh Wurman (OU) and Jerry Straka (OU) also provided real-time information; the former also graciously shared his team's DOW data, which David Dowell provided. Mark Laufersweiler (OU) assisted with computer-related issues. We are indebted to John Snow, Rich Rotunno, David Nolan, and Kerry Emanuel for discussions about vortex dynamics. This project was funded by NSF Grants ATM-9612674 and -9912097 to OU and by ATM-9616730 to the University of Massachusetts—Amherst. The first author was a visitor on sabbatical leave in the Mesoscale and Microscale Meteorology Division of the National Center for Atmospheric Research (NCAR) during the final part of this study. NCAR is supported by the National Science Foundation.

REFERENCES

Atkins, N. T., M. L. Weisman, and L. J. Wicker, 1999: The influence of preexisting boundaries on supercell evolution. *Mon. Wea. Rev.,* **127,** 2910–2927.

Barcilon, A., and P. G. Drazin, 1972: Dust devil formation. *Geophys. Fluid Dyn.,* **4,** 147–158.

Bluestein, H. B., 1999: A history of storm-intercept field programs. *Wea. Forecasting,* **14,** 558–577.

——, and A. L. Pazmany, 2000: Observations of tornadoes and other convective phenomena with a mobile, 3-mm wavelength, Doppler radar: The spring 1999 field experiment. *Bull. Amer. Meteor. Soc.,* **81,** 2939–2951.

——, W. P. Unruh, J. LaDue, H. Stein, and D. Speheger, 1993: Doppler radar wind spectra of supercell tornadoes. *Mon. Wea. Rev.,* **121,** 2200–2221.

——, A. L. Pazmany, J. C. Galloway, and R. E. McIntosh, 1995: Studies of the substructure of severe convective storms using a mobile 3-mm wavelength Doppler radar. *Bull. Amer. Meteor. Soc.,* **76,** 2155–2169.

——, S. G. Gaddy, D. C. Dowell, A. L. Pazmany, J. C. Galloway, R. E. McIntosh, and H. Stein, 1997a: Mobile, 3-mm wavelength, pulsed Doppler radar observations of substorm-scale vortices in a supercell. *Mon. Wea. Rev.,* **125,** 1046–1059.

——, W. P. Unruh, D. C. Dowell, T. A. Hutchinson, T. M. Crawford, A. C. Wood, and H. Stein, 1997b: Doppler radar analysis of the Northfield, Texas, tornado of 25 May 1994. *Mon. Wea. Rev.,* **125,** 212–230.

——, W.-C. Lee, M. Bell, C. C. Weiss, and A. L. Pazmany, 2003: Mobile Doppler radar observations of a tornado in a supercell near Bassett, Nebraska, on 5 June 1999. Part II: Tornado-vortex structure. *Mon. Wea. Rev.,* **131,** 2968–2984.

Brandes, E. A., 1978: Mesocyclone evolution and tornadogenesis: Some observations. *Mon. Wea. Rev.,* **106,** 995–1011.

Brown, R. A., and V. T. Wood, 1991: On the interpretation of single-Doppler velocity patterns within severe thunderstorms. *Wea. Forecasting,* **6,** 32–48.

Davies-Jones, R., R. J. Trapp, and H. B. Bluestein, 2001: Tornadoes and tornadic storms. *Severe Convective Storms, Meteor. Monogr.,* No. 50, Amer. Meteor. Soc., 167–221.

Doviak, R. J., and D. Sirmans, 1973: Doppler radar with polarization diversity. *J. Atmos. Sci.,* **30,** 737–738.

Dowell, D. C., and H. B. Bluestein, 1997: The Arcadia, Oklahoma, storm of 17 May 1981: Analysis of a supercell during tornadogenesis. *Mon. Wea. Rev.,* **125,** 2562–2582.

——, and ——, 2002a: The 8 June 1995 McLean, Texas, storm. Part I: Observations of cyclic tornadogenesis. *Mon. Wea. Rev.,* **130,** 2626–2648.

——, and ——, 2002b: The 8 June 1995 McLean, Texas, storm. Part II: Cyclic tornado formation, maintenance, and dissipation. *Mon. Wea. Rev.,* **130,** 2649–2670.

Drazin, P. G., and L. N. Howard, 1966: Hydrodynamic stability of parallel flow of inviscid fluid. *Advances in Applied Mechanics,* G. G. Chernyi, Ed, Vol. 9, Academic Press, 1–89.

Fujita, T. T., 1981: Tornadoes and downbursts in the context of generalized planetary scales. *J. Atmos. Sci.,* **38,** 1511–1534.

Lee, B. D., and R. B. Wilhelmson, 1997a: The numerical simulation of nonsupercell tornadogenesis. Part I: Initiation and evolution of pretornadic misocyclone circulations along a dry outflow boundary. *J. Atmos. Sci.,* **54,** 32–60.

——, and ——, 1997b: The numerical simulation of nonsupercell tornadogenesis. Part II: Evolution of a family of tornadoes along a weak outflow boundary. *J. Atmos. Sci.,* **54,** 2387–2415.

Lemon, L. R., and C. A. Doswell, 1979: Severe thunderstorm evolution and mesocyclone structure as related to tornadogenesis. *Mon. Wea. Rev.,* **107,** 1184–1197.

Lewellen, D. C., and W. S. Lewellen, 2002: Near-surface intensification during unsteady tornado evolution. Preprints, *21st Conf. on Severe Local Storms,* San Antonio, TX, Amer. Meteor. Soc., 481–484.

——, and ——, J. Xia, 2000a: The influence of a local swirl ratio on tornado intensification near the surface. *J. Atmos. Sci.,* **57,** 527–544.

——, ——, and ——, 2000b: Nonaxisymmetric, unsteady tornadic corner flows. Preprints, *20th Conf. on Severe Local Storms,* Orlando, FL, Amer. Meteor. Soc., 265–268.

Lewellen, W. S., and D. C. Lewellen, 1997: Large-eddy simulation of a tornado's interaction with the surface. *J. Atmos. Sci.,* **54,** 581–605.

Lhermitte, R. M., 1990: Attenuation and scattering of millimeter wavelength radiation by clouds and precipitation. *J. Atmos. Oceanic Technol.,* **7,** 464–479.

Markowski, P. M., 2002: Hook echoes and rear-flank downdrafts: A review. *Mon. Wea. Rev.,* **130,** 852–876.

Nettleton, L. S., S. Daud, R. Neitzel, C. Burghart, W.-C. Lee, and P. Hildebrand, 1993: SOLO: A program to peruse and edit radar data. Preprints, *26th Conf. on Radar Meteorology,* Norman, OK, Amer. Meteor. Soc., 338–339.

Pazmany, A. L., J. C. Galloway, J. B. Mead, I. Popstefanija, R. E. McIntosh, and H. B. Bluestein, 1999: Polarization diversity pulse-pair technique for millimeter-wave Doppler radar measurements of severe storm features. *J. Atmos. Oceanic Technol.,* **16,** 1900–1911.

Ray, P. S., B. C. Johnson, K. W. Johnson, J. S. Bradberry, J. J. Stephens, K. K. Wagner, R. B. Wilhelmson, and J. B. Klemp, 1981: The morphology of several tornadic storms on 20 May 1977. *J. Atmos. Sci.,* **38,** 1643–1663.

Rotunno, R., 1984: An investigation of a three-dimensional asymmetric vortex. *J. Atmos. Sci.,* **41,** 283–298.

Trapp, R. J., 1999: Observations of nontornadic low-level mesocyclones and attendant tornadogenesis failure during VORTEX. *Mon. Wea. Rev.,* **127,** 1693–1705.

Wakimoto, R. M., and J. W. Wilson, 1989: Nonsupercell tornadoes. *Mon. Wea. Rev.,* **117,** 1113–1140.

——, and B. E. Martner, 1992: Observations of a Colorado tornado. Part II: Combined photogrammetric and Doppler radar analysis. *Mon. Wea. Rev.,* **120,** 522–543.

——, and N. T. Atkins, 1996: Observations on the origins of rotation: The Newcastle tornado during VORTEX 94. *Mon. Wea. Rev.,* **124,** 384–407.

——, and C. Liu, 1998: The Garden City, Kansas, storm during VORTEX 95. Part II: The wall cloud and tornado. *Mon. Wea. Rev.,* **126,** 393–408.

——, and H. Cai, 2000: Analysis of a nontornadic storm during VORTEX 95. *Mon. Wea. Rev.,* **128,** 565–592.

——, C. Liu, and H. Cai, 1998: The Garden City, Kansas, storm during VORTEX 95. Part I: Overview of the storm's life cycle and mesocyclogenesis. *Mon. Wea. Rev.,* **126,** 372–392.

Weisman, M. L., and J. B. Klemp, 1982: The dependence of numerically simulated convective storms on vertical wind shear and buoyancy. *Mon. Wea. Rev.,* **110,** 504–520.

Wicker, L. J., and R. B. Wilhelmson, 1995: Simulation and analysis of tornado development and decay within a three-dimensional supercell thunderstorm. *J. Atmos. Sci.,* **52,** 2675–2703.

Wurman, J., and S. Gill, 2000: Finescale radar observations of the Dimmitt, Texas (2 June 1995), tornado. *Mon. Wea. Rev.,* **128,** 2135–2164.

——, J. M. Straka, E. N. Rasmussen, M. Randall, and A. Zahrai, 1997: Design and deployment of a portable, pencil-beam, pulsed, 3-cm Doppler radar. *J. Atmos. Oceanic Technol.,* **14,** 1502–1512.

Ziegler, C. L., E. N. Rasmussen, T. R. Shepherd, A. I. Watson, and J. M. Straka, 2001: The evolution of low-level rotation in the 29 May 1994 Newcastle–Graham, Texas, storm complex during VORTEX. *Mon. Wea. Rev.,* **129,** 1339–1368.